

Systematic Variation in Galena Solid-Solution Compositions at Santa Eulalia, Chihuahua, Mexico

VIRGIL W. LUETH,[†]

New Mexico Bureau of Mines and Mineral Resources, Socorro, New Mexico 87801

PETER K.M. MEGAW,

IMDEX, Inc., Tucson, Arizona 85728

NICHOLAS E. PINGITORE, AND PHILIP C. GOODELL

Department of Geological Sciences, University of Texas at El Paso, El Paso, Texas 79968

Abstract

Argentiferous galena is the main silver-bearing phase at both the East and West camps of the Santa Eulalia district, Chihuahua, Mexico. The silver occurs as a coupled substitution of Ag and Sb for Pb in PbS with compositions ranging from 0.04 to 5.9 atomic percent (at. %) Ag and 0.10 to 7.2 at. percent Sb. Correlation analysis between Ag and Sb resulted in *r* values of 0.97 and 0.99 (significant at the 98% confidence level) for direct-current plasma-atomic emission spectroscopy (DCP-AES) and microprobe analysis of galena, respectively. Discrete and crystallographically oriented inclusions of diaphorite (usually 1 μm or smaller) were common in high silver-antimony galenas and rare in low silver types (when present, tend to be larger). These inclusions were most abundant in the core zones of the crystals and rare on the edges.

Spatial and temporal variations in Ag-Sb concentrations and ratios in galena were found mainly in the West camp of the district. High silver galenas (maximum 5.9 at. %) are confined to skarn zones or deep manto and chimney areas. The Ag/Sb ratio increases in galena from depth (0.88) to the surface (1.04) and from south (0.76) to north (0.94), following zonation and flow patterns established in previous investigations. Differences in Ag-Sb substitution in galena are also seen in different mineralization types: breccia zones, deep mantos, and chimneys contain more Ag-Sb (3.5 at. % avg) and have lower Ag/Sb ratios (avg ratio = 0.88) than the upper mantos, silicate and calc-silicate orebodies, which have lower Ag-Sb concentrations (2.2 avg at. %) but higher ratios (avg ratio = 1.00).

Silver and antimony substitution also correlates with sulfur isotope variation in the district. Within individual orebodies, the $\delta^{34}\text{S}$ value increases with decreasing silver and antimony concentrations in galena. The solid-solution compositional variations in galena coupled with sulfur isotope values are a useful tool for inferring fluid paths and appear to reflect fluid evolution.

At Santa Eulalia, silver is disseminated to various degrees throughout the orebodies and galena solid-solution concentrations appear to be controlled by subtle physical and/or chemical gradients. This contrasts with volcanic-epithermal systems in which significant physiochemical perturbations (large thermal and pressure gradients, boiling, etc.) lead to dumping of precious metals and semimetals as sulfosalts in bonanza zones. Relatively low concentrations of other potential ore-forming elements, namely copper and bismuth, also precluded the formation of a complex suite of silver sulfosalts and antimonian-argentiferous galena precipitated instead. Sulfosalts at Santa Eulalia are localized to upper mineralized zones as breccia void fillings, indicative of limited zones of boiling.

Introduction

ARGENTIFEROUS galena is reported to be the main silver-bearing phase at both the East and West camps of the Santa Eulalia mining district of northern Mexico (Fig. 1). Other silver-bearing phases include minor acanthite and rare occurrences of fizelyite, argentopyrite, freibergite, native silver, proustite, pyrrargyrite, stephanite, tennantite-tetrahedrite, and polybasite (Megaw, 1986a, 1990). In order to incorporate significant amounts of silver into galena, a coupled substitution with antimony or bismuth is required (Van Hook, 1960; Hoda and Chang, 1975; Amcoff, 1976; Foord and Shave, 1988). The coupled substitution, $\text{Ag}^+ + \text{Sb}^{3+}$ for 2Pb^{2+} , maintains charge balance and its maximum extent is controlled by temperature, silver and antimony activity, the concentrations of other metal

ions which are capable of forming sulfosalts (Amcoff, 1984), or a combination of these factors. The mineralization at Santa Eulalia provides an opportunity to study coupled substitution of silver and antimony in galena hosted by skarn and manto ores.

Previous studies of the district are extensive and best summarized in publications by Prescott (1916, 1926), Hewitt (1943, 1968), and Megaw et al. (1988). Bond (1986) and Walter (1985) studied mineralogical, geochemical, and metal zoning at the San Antonio mine in the East camp and their results were incorporated into this study. A dissertation by Megaw (1990) provides the most detailed modern study of the district. The samples for this study are the same ones used by Megaw (1990). Lueth et al. (1996) first documented compositional variations in galena at the West camp of the Santa Eulalia district.

[†] Corresponding author: email, vwlueth@nmt.edu

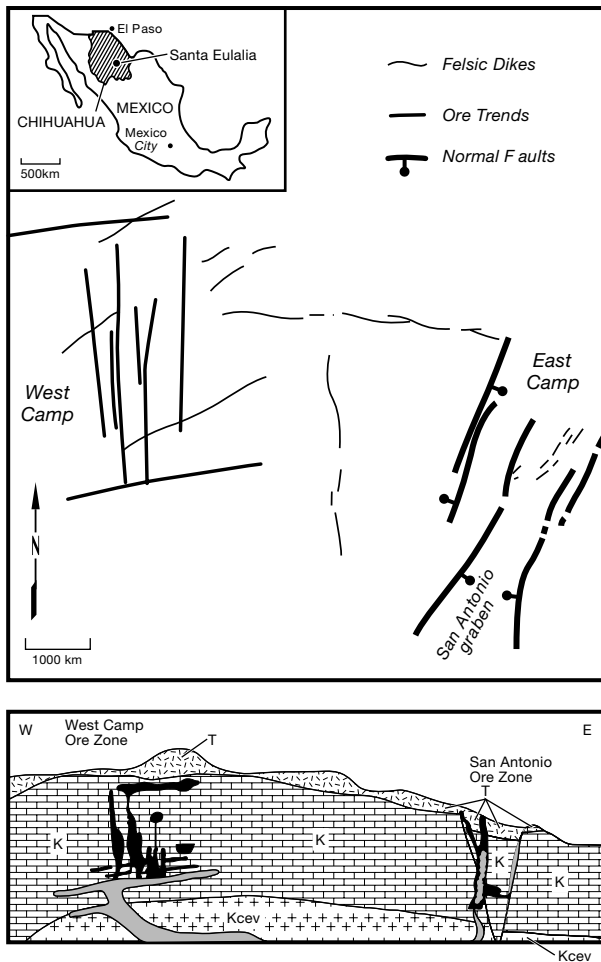


FIG. 1. Location map, generalized geologic plan map, and generalized geologic cross section of the Santa Eulalia district. Geologic cross section illustrates the geologic relationships within the deposits. Symbols: K = undifferentiated Cretaceous sedimentary rocks, Kcev = Cretaceous evaporite deposits, Kf = felsite dikes and sills, T = undifferentiated Tertiary volcanic rocks. Orebodies are depicted as irregularly shaped black masses in the cross section. Geology modified from Megaw (1990).

Summary of the Geology of the District

General geology

The geologic setting of the Santa Eulalia district is similar to other high-temperature, carbonate-hosted Ag-Pb-Zn deposits of northern Mexico (Megaw et al., 1988). The host rocks are Cretaceous limestones intruded by felsite and diabase dikes and sills (Fig. 1). Mineralization is associated in time and space with the felsite intrusions in two zones known as the East and West camps, which lie on opposite flanks of a broad, doubly plunging anticline. The felsites are texturally and compositionally indistinguishable and have identical REE patterns (Megaw, 1990). West camp mineralization consists of massive sulfide mantos and chimneys with lesser mineralized breccias and skarn bodies. East camp mineralization consists of dike contact skarns with subordinate massive sulfide bodies. Structural controls on mineralization in both camps include reactivated fold-related fracturing and faulting as well as intrusive contacts. Host-rock lithology (especially

secondarily enhanced permeability) controls ore distribution in the upper and peripheral parts of the district. Ten different ore types have been recognized in the district (Table 1), but only the normal sulfides, silicates (calcic-iron skarns), and calc-silicate skarn ores (Hewitt, 1968; Megaw, 1990) were examined in this study. The ore mineralogy throughout the district is relatively simple, consisting of pyrrhotite, pyrite, sphalerite, and galena with minor amounts of calcite, quartz, fluorite and, in places, calc-silicate gangue. Despite stark differences in trace metal contents and the amount and composition of the skarns in the two camps, the overall geologic character, fluid inclusion compositions, sulfur, oxygen and carbon isotope characteristics, and alteration assemblages are similar enough to indicate that the ore fluids for both camps had a common origin (Megaw, 1990).

West camp mineralization

Manto and chimney deposits are the most common types of mineralization in the West camp. The ore mineralogy consists of pyrrhotite, galena, sphalerite, and pyrite, replacing limestone with little alteration of the host rock. Skarn mineralization is more limited, present as either silicate or calc-silicate orebodies. Silicate orebodies consist of Ca-Fe silicates with Mn-rich compositions. The silicate orebodies are reported to have higher silver values than the manto ores (Prescott, 1916). Calc-silicate orebodies consist of calcic skarn silicate minerals and an ore assemblage of galena, sphalerite, arsenopyrite, pyrite, and pyrrhotite. Trace amounts of chalcopyrite and pyrrhotite occur as inclusions in sphalerite. Acanthite, pyrargyrite, argentopyrite, polybasite, and stephanite are also reported as discrete minerals in the calc-silicate ores (Megaw, 1990).

East camp mineralization

Mineralization in the East camp is controlled by structures related to the San Antonio graben (Fig. 2) and the contacts of a series of felsite dikes that follow and cut across the graben faults (Hewitt, 1943). Skarn mineralization dominates and calc-silicate mineralogy is bilaterally and symmetrically zoned outward from the dikes. The dikes are widely converted to calc-silicates (Megaw, 1990). Most of the sulfides in the East camp occur within the skarn, but podiform sphalerite + pyrite \pm pyrrhotite bodies (\pm galena) commonly occur between the skarns and the enclosing limestone. Massive sulfide mantos composed of galena, sphalerite, and pyrrhotite, texturally similar to the West camp ores, occur in contact with, and peripheral to, the skarns.

Methodology

Samples utilized for this study were the same materials collected and analyzed by Megaw (1990), and detailed sample locations and descriptions can be found there. Bulk chemical analyses of the galena by direct-current plasma-atomic emission spectroscopy (DCP-AES) were performed on the sulfur isotope samples. Petrographic samples were analyzed by electron microprobe. Figures 2 and 3 provide generalized location maps for the samples. Galena samples were digested by the method described in Rubeska et al. (1967). The mineral (0.1 g) was dissolved in 6 ml of 1M nitric acid and 10 ml of 10 percent (w/v) tartaric acid overnight and then heated to near

TABLE 1. Types of Mineralization in the East and West Camps, Santa Eulalia, Chihuahua, Mexico

Mineralization type ¹	Sulfide mineralogy	Gangue mineralogy	Trace metals	Deposit types	Important ore-bodies
West camp mineralization					
Normal sulfides	Pyrrhotite, pyrite, sphalerite, galena, rare tetrahedrite	Calcite, dolomite minor fluorite, quartz in upper zones	Silver, antimony	Mantos and chimneys	85% of West camp production
Silicate ores	Pyrrhotite, pyrite, sphalerite, galena	Manganooan-fayalite, manganooan-clinopyroxene, ilvaite, hisingerite, chlorite, rhodochrosite, quartz, fluorite	Silver tin, tungsten, boron	Mantos, chimneys, breccias	Buena Tierra mine (Penoles trend), Velardena shaft, Inglaterra silicate, Main silicate, Tunnel
Calc-silicate skarn	Galena, sphalerite, arsenopyrite, pyrite, pyrrhotite, chalcopyrite, acanthite, pyrrarygyrite, stephanite	Tremolite, actinolite, diopside, garnet, manganooan-calcite, fluorite, rhodonite, pyroxmangite	Silver, arsenic, copper, antimony	Chimneys	Matona chimney
Veinlet	Galena, sphalerite, pyrrhotite	Calcite	None reported	Veins and veinlets	Tops of most orebodies, extending into limestone
Gypsum ores	Pyrite, sphalerite, galena	Gypsum, fluorite	None reported	Mantos and chimneys	West, Ventura, Roy, Tunnel, Main Silicate
Disseminated mineralization	Pyrite, sphalerite, galena	Calcite, host limestone	None reported	Disseminated	Adjacent to major orebodies
East camp mineralization					
Calc-silicate skarn	Pyrrhotite, pyrite, sphalerite, galena, rare tetrahedrite	Epidote, chlorite, garnet, hedenbergite, diopside, tremolite, seapolite, actinolite, cummingtonite, q ilvaite, fluorite, vesuvianite, quartz	Silver, cadmium, indium, bismuth, gold	Mantos and chimneys	Majority of East camp production
Normal sulfide	Sphalerite, pyrite, pyrrhotite, galena, arsenopyrite, chalcopyrite, acanthite, marcasite, cinnabar, stibnite, realgar, orpiment	Manganooan-fayalite, manganooan-clinopyroxene, ilvaite, hisingerite, chlorite, rhodochrosite, quartz, fluorite	Silver, copper	Mantos, pods	20% of East camp production
Tin-bearing ores	Cassiterite, silver-lead oxides, lead-vanadium oxides, ilmenite, hematite, magnetite, columbite, wolframite, franklinite	Garnet, tremolite, hedenbergite, jasperoid, fluorite, muscovite, tourmaline, topaz, orthoclase	Silver, vanadium, tungsten	Chimneys, fissures	Tin chimney, Cock's orebody, Dolores fissures
Veinlet	Magnetite, franklinite, pyrrarygyrite, proussite, hematite,	Calcite, quartz, fluorite	None reported	Veins and veinlets	Throughout mineralized interval
Oxide ores	Cerussite, anglesite, hemimorphite, smithsonite	Iron oxides, manganese oxides, calcite, quartz, fluorite, gypsum	None reported	Mantos and chimneys	Above water table

¹ Classification of Megaw (1990)

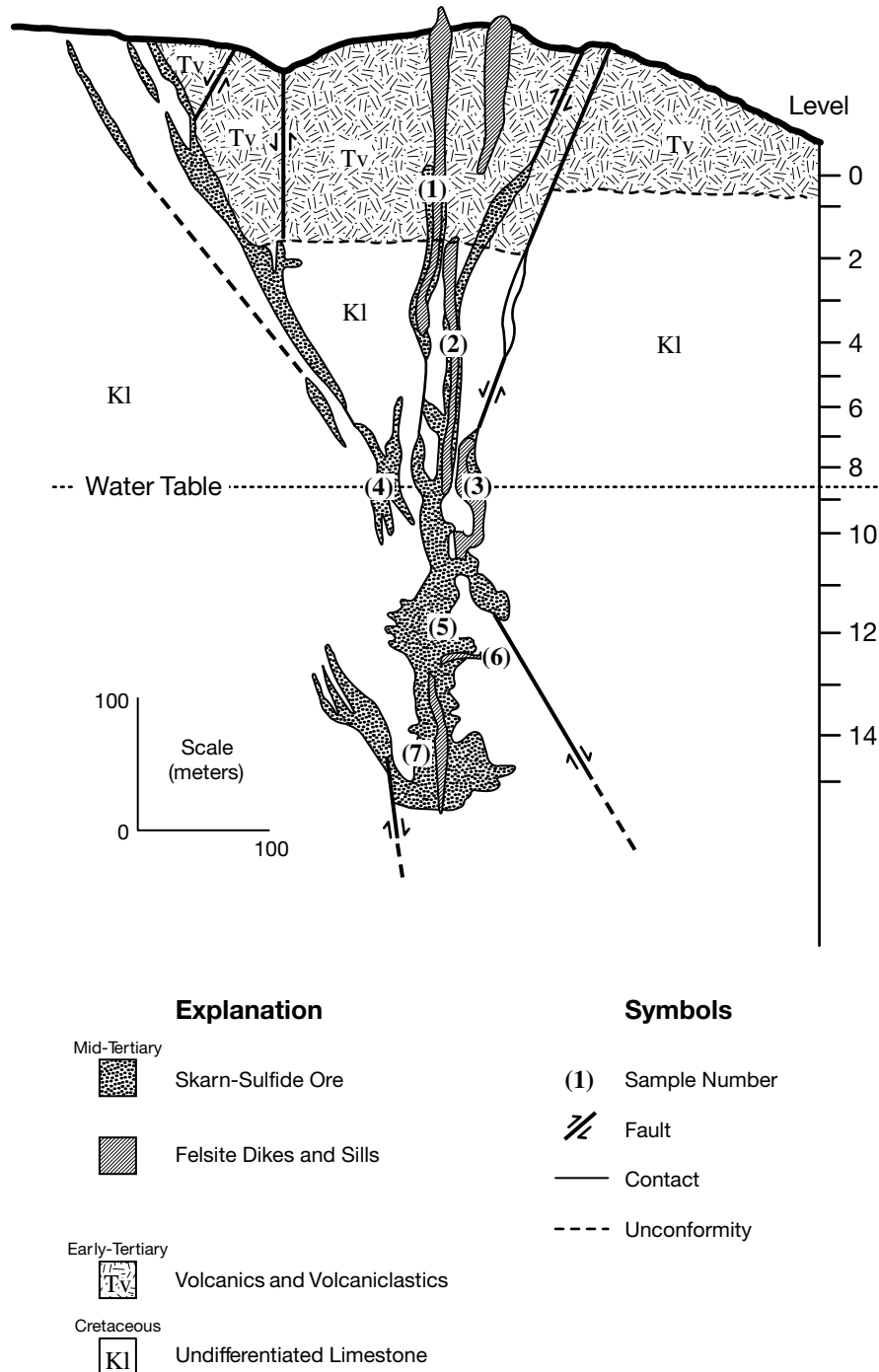


FIG. 2. Cross section of the San Antonio mine, illustrating sample locations for DCP-AES samples. Cross section modified from Bond (1986).

boiling for 2 h. Three milliliters of mercury (II) nitrate solution (10 mg Hg/ml) were added to the dissolved galena solution to prevent precipitation of silver chloride. The liquid was filtered and the filtrate washed and decanted twice. The volume of the filtrate was then brought to 100 ml in a volumetric flask with deionized water. The samples were stored in polypropylene bottles until analyses were performed (2 d max storage time before analysis for all elements). Galena solutions

were analyzed on a direct-current plasma-atomic emission spectroscope at the University of Texas at El Paso. After initial calibration, standards were interspersed with samples and a limited number of unknown samples were run multiple times to check accuracy and reproducibility.

Standards were prepared in a matrix similar to that of natural galenas. Standard solutions of Ag, Sb, Bi, and Pb (1,000 mg/l) were made by dissolving appropriate sulfides of 99.999

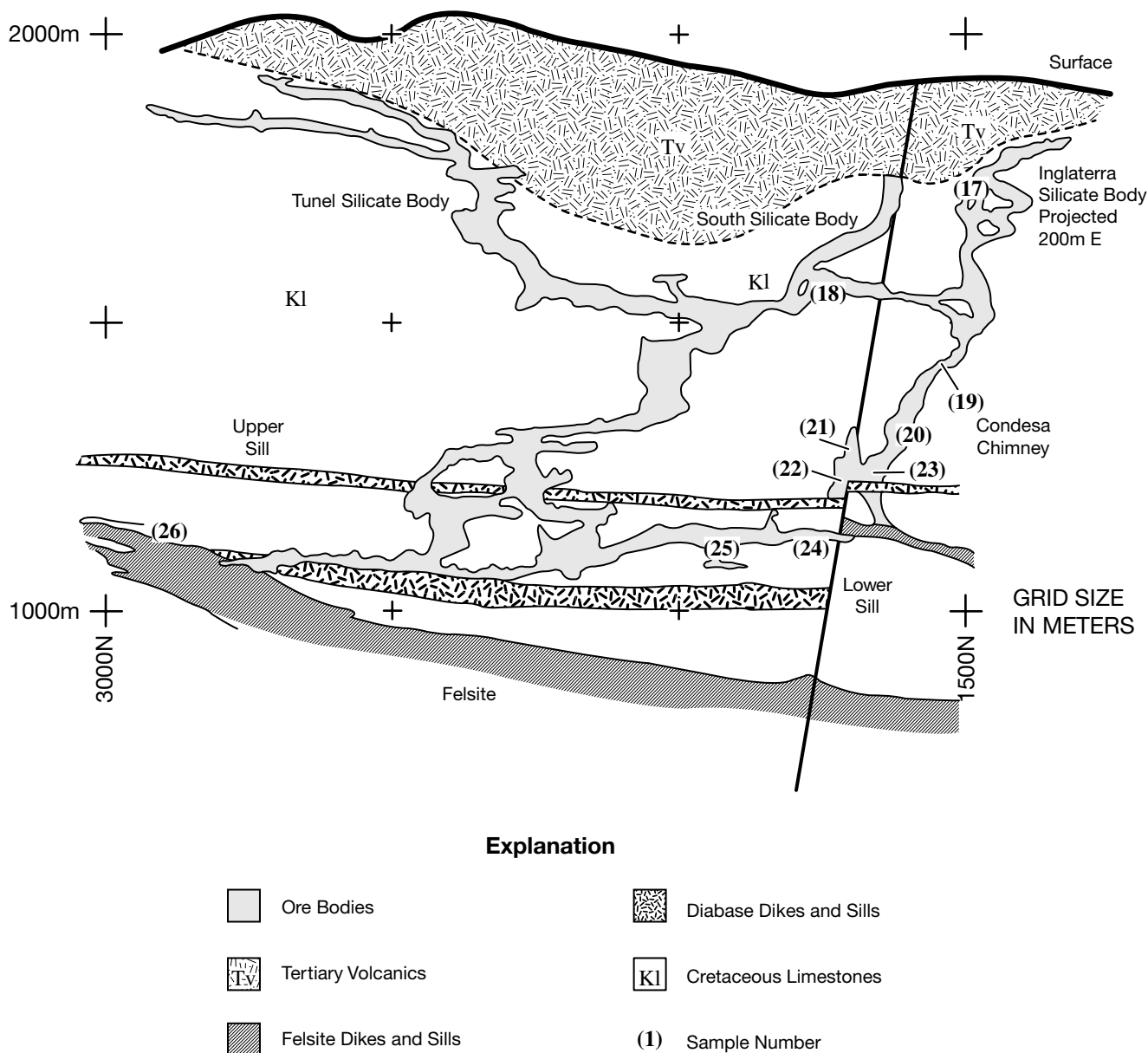


FIG. 3. Longitudinal section, looking east along N 10° W-trending Tiro Alto-Q-Denis trend with sample locations projected onto section. Section modified from Megaw (1990).

percent purity into the same acid solutions as those described above. The 1,000 mg/l PbS solution was used to dilute the Ag, Sb, and Bi standards to maintain proper matrix characteristics. A standard range of 100, 10, 1, and 0.1 mg/l for each element was made by successive dilutions. This standard range represents a range of compositions in galena of 10, 1, 0.1, and 0.01 at. percent. A similar concentration range for As, Se, and Te was prepared from commercially purchased stock solutions.

Five replicate analyses of 0.1 at. percent (in galena) standards of Ag, Sb, Bi, As, and Se run during the course of analysis of the unknowns yielded standard deviations of 0.03, 0.08, 0.17, 0.32, and 0.15 (at. %) for the respective elements. Tellurium was undetectable in the samples. The larger standard

deviations for Bi and As reflect analysis near the detection limit for the instrument. Detection limits for the elements in galena samples were as follows: Ag = 0.004, Sb = 0.008, Bi = 0.002, As = 0.008, Se = 0.01, and Te = 0.02 at. percent.

Polished thin sections from ores at some of the sample locations were examined for optically recognizable mineral inclusions to a maximum magnification of 400x. Petrographic samples of galena from Megaw (1990) were analyzed by electron microprobe. Fluid inclusion and sulfur isotope data from Megaw (1990) were compared to the results from this study.

Electron microprobe analyses were performed on two instruments. Wavelength dispersion analysis was performed on a Cameca SX-50 instrument at the University of Texas at El Paso. Grains were analyzed by individual spot analysis along

grain traverses from the center of the grain to the edges. All corrections were made using PAP algorithms (Pouchou and Pichoir, 1984). On grains other than galena, energy dispersive spectroscopy analyses were performed and compositions determined by standardless analysis. Backscatter imaging and X-ray mapping were performed on a Cameca SX-100 at the New Mexico Bureau of Mines and Mineral Resources using similar settings. The second instrument was capable of resolving backscatter images of inclusions in the galena to slightly less than 1 μm .

Analytical Results

DCP-AES analysis of galena

All 26 samples analyzed contained silver and antimony in measurable amounts (Table 2). Values of Ag and Sb in galena ranged from 0.8 to 6.2 at. percent Ag and 0.5 to 5.6 at. percent Sb. Silver and antimony values were nearly equal in the

galena samples with two exceptions (Fig. 4 and Table 2). Sample 25 proved not to be pure galena; the low lead content and high silver and antimony concentrations suggests that it was a silver-antimony sulfosalt, probably tetrahedrite. Sample 8 was very high in silver and low in antimony or bismuth, indicating the possible inclusion of acanthite in the sample. Bismuth was detected in only three samples, two from the San Antonio mine in the East camp and one from a deep level of the West camp. Arsenic was detected in all but three samples and selenium was detected in six samples. Most arsenic and selenium values were barely over the detection limit for the elements. Tellurium was not detected in any samples. Analysis results were plotted on mine maps for the East (Bond, 1986) and West (Megaw, 1990) camps. All data from DCP-AES analyses represent sampling of entire grains and were used to determine district zoning patterns.

East camp samples: Compositional variation in galena (Table 2) in the East camp displays no distinctive pattern with depth.

TABLE 2. Galena Compositions and Sulfur Isotope Values from Santa Eulalia, Mexico

No. ¹	Reference no. ²	Ore type	Ag	Sb	Bi	As	Se	Ag/Sb	$\delta^{34}\text{S}^3$
East camp samples									
1	SA 0	Oxidized skarn	2.8	2.6		0.1	tr	1.08	-9.22
2	SA 4	Oxidized skarn	0.9	0.9		0.3		1.00	2.84
3	SA 8	2350N Skarn	4.3	4.2				1.02	-10.57
4	SA 8 1725N	Manto	2.2	2.5	0.4	tr		0.88	-3.29
5	SA 13R 29 S	Skarn	3.1	3.5				0.88	4.20
6	SA 13R 29 M	Manto	1.7	1.7		0.1	0.1	1.00	-10.67
7	SA 14R 200N	Skarn	2.3	2.2	0.8	0.1		1.04	-11.82
West camp samples									
Northern West camp									
8	Parc Bx-1	Oxidized manto	6.2	0.5		0.2		12.40	-8.40
Matona chimney									
9	EP 21 U	Chimney	3.1	2.7	0.9	0.3		1.14	-10.78
Central West camp (listed from shallow levels to depth)									
10	BT-2 Ch	Chimney	1.7	1.9				0.89	-11.02
11	BT-4	Manto	0.8	0.9		0.2		0.88	-0.87
12	EP 10-CS-2	Silicate	1.6	0.9		0.1		1.70	-9.74
13	EP 15-C—C	Chimney	2.4	2.5		0.3		0.96	-9.74
14	BT-16-Ch	Chimney	2.7	2.8		0.3		0.96	-8.59
15	BT-20 PEN	Manto	1.6	2.1		0.2		0.76	-11.82
16	BT-21 JN	Manto	1.9	1.9		0.3	0.2	1.00	-9.78
Condesa fracture (listed from shallow levels to depth)									
17	Ingl-2-3	Silicate	2.4	2.3		0.2		1.04	-14.73
18	EP-10 C/Q	Silicate	2.0	2.0		0.7		1.00	-14.83
19	EP-16	Chimney	3.0	2.8		0.3	0.1	1.07	-15.35
20	EPCond 18-3	Chimney repl.	2.3	2.6		0.3	tr	0.88	-14.10
21	EPCond 19+	Chimney repl.	2.3	2.2		0.4		1.04	-13.62
22	2EP 19-2	Chimney bx	3.0	3.4		0.1		0.88	-16.18
23	EP 19 DS	Manto	5.2	5.6		0.1		0.92	-14.73
Q-Denis fracture (listed from Condesa breccia area northward)									
24	EP 20 Q900S	Manto	2.3	3.0		0.2		0.76	-15.83
25	EP 20 Q700S	Manto	5.9	7.2		0.1		0.82	-15.35
26	EP 20 Q50N	Manto	1.7	1.8		0.1	0.2	0.94	-11.29

¹ Sample number used in this study

² Sample number of Megaw (1990)

³ From Megaw (1990)

All compositions determined by direct coupled plasma-atomic emission spectroscopy (DCP-AES); values reported for Ag and Sb as at. percent in galena

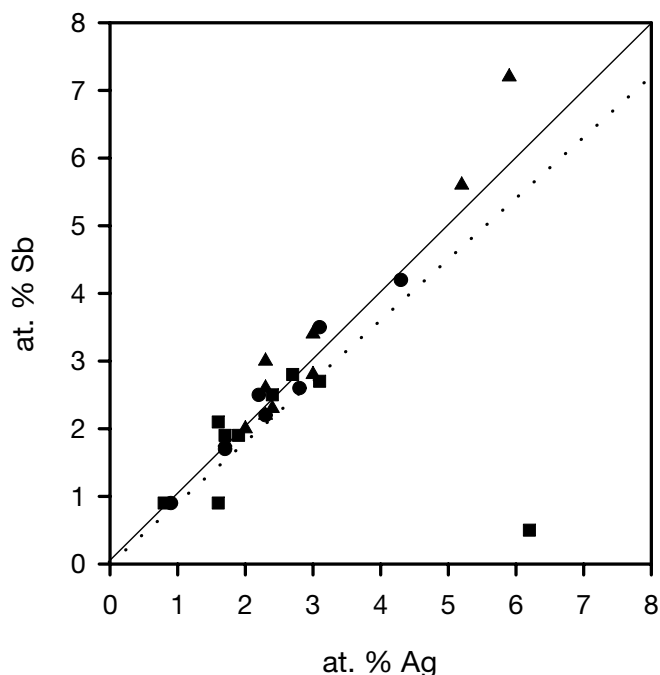


FIG. 4. Plot of at. percent Ag vs. Sb in galenas from Santa Eulalia, Chihuahua, Mexico, determined by DCP-AES analysis. Symbol size represents analytical error. Symbols: ● = East camp samples, ■ = northern and central West camp samples, ▲ = Condesa trend and southern West camp samples. Solid line represents a theoretical 1/1 coupled substitution. Dashed line represents a regression line fit to the data, with an r value of 0.94.

Most samples analyzed were from skarn ores. The highest silver and antimony values are present in samples from level 8. Bismuth was detected in two samples from skarn ores (7 = 0.8 and 4 = 0.4 at. %). The highest arsenic values (0.3 at. %) were found in samples above mine level 8. A selenium value of 0.01 at. percent (the detection limit) was found at level 13 of the San Antonio mine. Variation in compositions was noted between the types of mineralization. Skarn ore galenas have higher silver values than manto samples. This is most readily apparent in samples from level 8 at the San Antonio mine. Skarn galena contained 4 at. percent Ag and Sb compared to 2.5 at. percent in the related manto ores.

West camp samples: Compositional variation in galena is more evident in the West camp and varies with depth and lateral position from the inferred source of the fluids and between mineralization types. Galena from chimney deposits tends to have higher concentrations of silver and antimony than the mantos, although samples from deep mantos are similar to chimneys. Galena samples from the deepest portions of the mines have Ag/Sb ratios less than 1, whereas samples from closer to the surface display values greater than 1 (Fig. 5). The range of the Ag/Sb ratio is 1.8 (south silicate body) to 0.76 (deep mantos and chimneys). Lower Ag/Sb ratios are especially evident in the Condesa region where the majority of the galena analyses have Ag/Sb ratios less than one. The uppermost orebodies analyzed in the West camp, the South silicate body, the Inglaterra silicate body, and the Parcionera manto have the highest Ag/Sb ratios in galena.

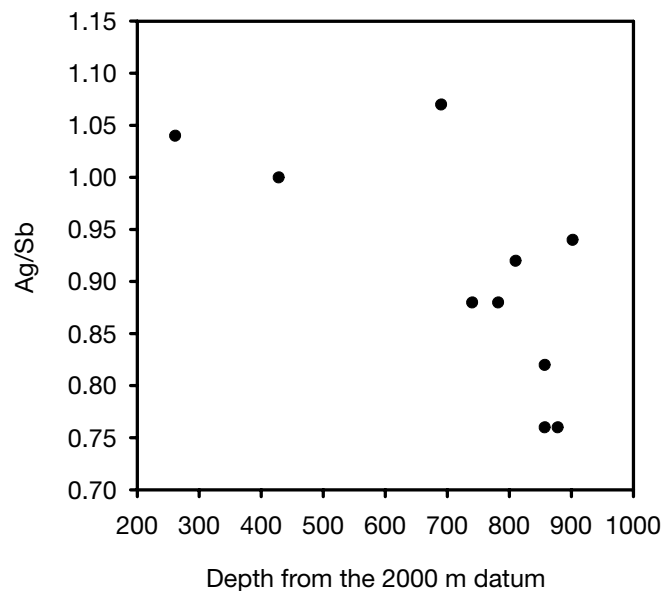


FIG. 5. Ag/Sb values for galena from the Condesa region compared to depth from an arbitrary datum near the surface. All values for ratio determinations by DCP-AES analysis.

Petrographic analysis of galena

Ore mineralogy is dominated by pyrrhotite, pyrite, sphalerite, and galena. Chalcopyrite is locally present and other sulfides are observed only in trace amounts (Megaw, 1990). Grain sizes vary significantly, between 1 mm and 5 cm, on local and orebody-wide scales. The largest grain sizes are associated with monomineralic sulfide layers in mantos and tend to be smallest in the chimneys and skarn orebodies. Fine-scale mineral banding was noted by Megaw (1990). Optically detectable inclusions in ore minerals are confined mainly to pyrrhotite in sphalerite and vice versa, and chalcopyrite disease. Megaw (1990) cited unpublished reports of occurrences of tennantite-freibergite and acanthite inclusions in galena from localized areas in the district. No optically detectable silver sulfide inclusions were noted in the samples studied. Acanthite pseudomorphs after argentite are reported but not common in the West camp. Discrete grains of native silver, pyrargyrite, argentopyrite, and polybasite were reported by Megaw (1986a) but are also uncommon. Silver and pyrargyrite are most abundant in the Tunel silicate body that is near the surface. The minerals occur in late breccia void infillings. Fizelyite is reported from surface outcrops of veinlets cutting the capping volcanics. These inclusions and discrete silver phases appear to be the exception in the district.

Textural relationships between the galena and other sulfides are consistent throughout the deposits. Textures are usually equant mosaic or interlocking between anhedral to subhedral grains. Replacement textures are dominated by mutual embayments between individual sulfide species (Megaw, 1990). The paragenetic relationships among the sulfide minerals are represented for both deposits in Figure 6. Open-space filling is not common in the district on a large scale and none of the samples used in this study displayed textures resulting from open-space deposition.

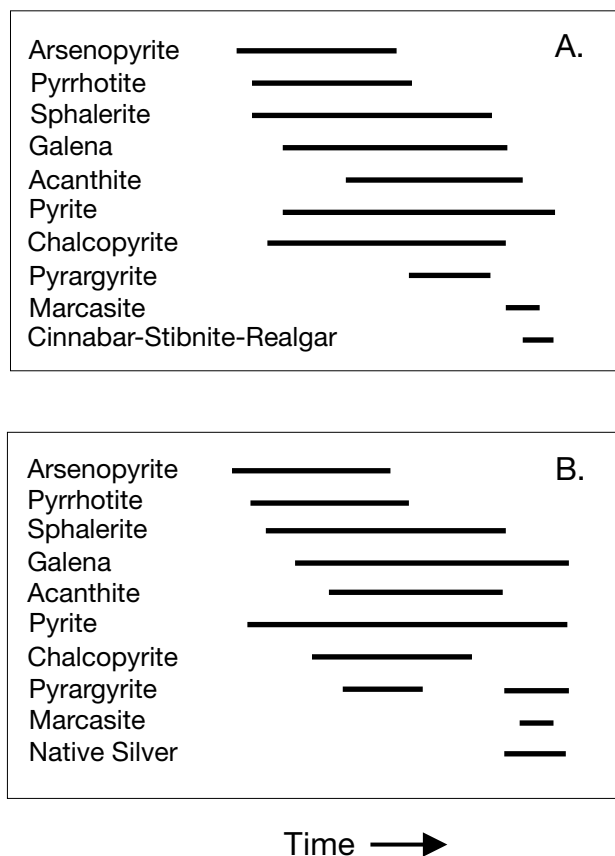


FIG. 6. Paragenesis diagrams for sulfide mineralization at Santa Eulalia. A. East camp. B. West camp. Diagram modified from Megaw (1990).

Electron microprobe analysis of galena

Discrete silver and antimony mineral inclusions in galena were observed in most of the ten samples analyzed by electron microprobe (Fig. 7). Individual tetrahedrite grains, associated with sphalerite, were also noted in samples from the East camp. Maximum concentrations encountered by electron microprobe analysis of Ag and Sb in galena were 1.78 and 1.69 at. percent, respectively. Most samples averaged 0.20 at. percent silver and antimony in zones free of inclusions. Eighty percent of all spot analyses (Table 3) contained less than 0.5 at. percent silver and antimony in contrast with the DCP-AES data in which all samples contained more than 0.5 at. percent Ag and Sb. This apparent discrepancy will be discussed later. A comparison of all galena microprobe analyses shows a consistent 1/1 at. ratio between Ag and Sb (Fig. 8). As silver and antimony increase, lead displays a corresponding decrease in concentration consistent with a coupled substitution into the galena structure, similar to the DCP-AES data.

Significant silver and antimony concentrations were observed in three types of discrete inclusions within individual galena grains (Fig. 7). The most common were oriented, rod-shaped inclusions of diaphorite confined to the centers of the

crystals (Fig. 9A and B). These inclusions varied in dimension with maximum lengths up to 10 μm and maximum observed diameters to 1 μm . The grain core zones consist of up to 5 percent diaphorite inclusions. Larger, elongated, and less regularly shaped (max observed length = 30 μm , max observed width = 20 μm) diaphorite grains were found isolated in the outer portions of some crystals (Fig. 9C and D). Diaphorite grains were lacking on the rims of galena grains and in those samples with Ag and Sb concentrations of less than 2.0 at. percent (Fig. 9E and F). A third type of inclusion, tetrahedrite grains, were encountered on the margins of galena grains usually associated with sphalerite (Fig. 7C and D) in samples from the East camp. Tetrahedrite grains displayed no consistent shape or crystallographic orientation within the galena grains in contrast to the diaphorite.

Average galena compositions determined by electron microprobe were lower in Ag and Sb than those concentrations determined by digestion and analysis by DCP-AES. Sampling bias (only 10 of the 26 samples were analyzed by microprobe) may contribute to the higher occurrence of low silver galenas in the microprobe analysis data. The samples used for DCP-AES and electron microprobe were not the same. However, the presence of oriented diaphorite in core zones in galena (up to 5% based on visual estimation) suggests the two-dimensional spot analysis of the galena does not often include the diaphorite inclusions. The bulk analysis of the galena grains by DCP-AES integrated the entire grain into the analysis and the presence of inclusions can account for the apparent discrepancy between the two methods within analytical error. However, the presence of argentian tetrahedrite in some samples would tend to skew that DCP-AES data toward higher Sb concentrations and cause lower apparent Ag/Sb ratios in the galena (e.g., samples 15, 24, and 25).

Sulfur isotope data

The sulfur isotope data used in this study were obtained by Megaw (1990). Sulfur isotopes from galena range between -16.18 to $+4.2$ per mil in the district for samples displaying evidence of isotopic equilibrium between galena and sphalerite. Megaw (1990) noted that evidence of isotopic disequilibrium between adjacent sulfide minerals is common. He also noted that no direct correlation was evident between sulfur isotopes and fluid inclusion temperatures, salinity, ore type, ore metal ratios, or iron sulfide species in either camp.

No consistent pattern was noted in the East camp. The $\delta^{34}\text{S}$ values in galena ranged from -11.82 to $+4.20$ per mil. The lack of any discernible isotopic pattern in the East camp was attributed to a more erratic and polyphase history of the deposit, typical of telescoped mineralization (Megaw, 1990).

A crude zoning pattern was seen with elevation, and distance from the deep southern chimney deposits of the West camp was noted by Megaw (1990). In the West camp, sulfur isotope values ranged from -15.83 to -0.87 per mil $\delta^{34}\text{S}$, with the most negative values in the vicinity of the southern chimneys and the least negative values in the upper and northern portions of the camp. Megaw (1990) suggests that a combination of varying initial $\delta^{34}\text{S}$ values and Rayleigh distillation is the best explanation for the range of sulfur isotope values and zoning in the West camp.

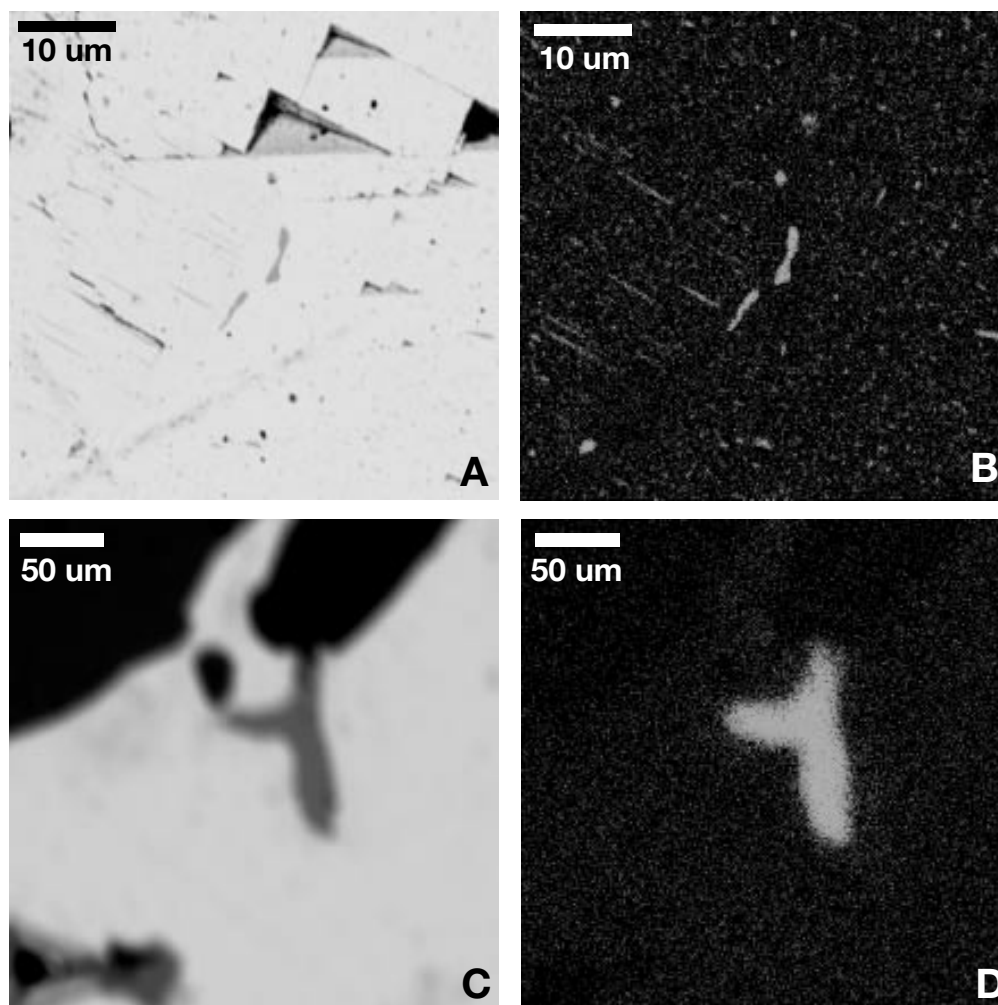


FIG. 7. Types of inclusions observed in galenas from the Santa Eulalia district. A. Backscatter image of oriented and un-oriented diaphorite inclusions in galena. B. Silver X-ray map of backscatter image in A. C. Backscatter image of tetrahedrite grain (medium gray) in galena (white) at the contact with sphalerite (black). D. Silver X-ray map of backscatter image C.

Discussion

Galena solid solution

Silver and antimony concentrations in the galena separates are consistent with a coupled substitution of Ag and Sb for Pb in PbS (Figs. 4 and 8). Correlation of DCP-AES and electron microprobe data indicates a strong coupling of Ag with Sb in the galena samples (r values of 0.97 and 0.99, significant at the 98% confidence level, respectively). All the galena analyses displaying evidence of coupled substitution of Ag and Sb for Pb in galena have similar compositional features noted by Malakov (1968), Amcoff (1976), Foord et al. (1988), Sharp et al. (1990), and Sharp and Buseck (1993).

Discrete sulfosalt inclusions were noted in the galenas analyzed from Santa Eulalia, similar to inclusions described by Sharp and Buseck (1993) in massive sulfide ores from La Paz, San Luis Potosi, and Concepcion del Oro, Zacatecas, Mexico. They attributed these rod-shaped and oriented inclusions of diaphorite to coherent exsolution at low temperatures. The consistent Ag/Sb ratio of approximately 1 would indicate that the silver and antimony were deposited as a solid solution in

galena, similar to those analyzed from Wood River, Idaho, by Hall and Czamanske (1972). The inclusion-rich core zones (Fig. 9A and B) may represent earlier formed galena grains that were later overgrown by galena with lower Ag-Sb concentrations.

Galena Ag/Sb values vary with concentration. Zones within galena grains of high Ag-Sb concentration have lower Ag/Sb ratios. Sharp and Buseck noted a slightly higher abundance of antimony over silver in samples from Zacatecas. They attributed this phenomenon to a greater solubility of Sb in the galena structure. This relationship holds true in the Condesa region of the West camp (Fig. 5). Lower Ag/Sb values (samples 20, 22, and 23) occur at depth and the ratio increases toward the surface (samples 17, 18, 19, and 21). This pattern may also reflect a higher Sb activity in the fluid at higher temperatures. Silver in galena is in greater proportions in the upper zones of the West camp at Santa Eulalia where Ag-Sb concentrations are lower. This may be a function of lower antimony activities in the upper zones of this deposit. In the areas where galenas display a higher proportion of silver relative to antimony, we speculate that the silver may be accommodated

TABLE 3. Galena Compositions Determined from Electron Microprobe Analysis of Galena Samples

Sample no.	<i>n</i>	Pb	Ag	Sb	S	Total	Ag/Sb	Atomic formula
2EP 20 Q700S	1	85.49	0.41	0.39	13.17	99.46	1.18	Pb _{49.49} Ag _{0.46} Sb _{0.39} S _{49.46}
	2	86.40	0.42	0.40	13.65	100.87	1.18	Pb _{49.07} Ag _{0.46} Sb _{0.39} S _{50.08}
	3	88.12	0.26	0.34	13.86	102.58	0.91	Pb _{48.28} Ag _{0.29} Sb _{0.32} S _{50.10}
	4	88.50	0.68	0.78	14.27	104.23	1.00	Pb _{48.28} Ag _{0.71} Sb _{0.71} S _{50.30}
	5	87.58	0.73	0.75	13.87	102.93	0.97	Pb _{48.67} Ag _{0.78} Sb _{0.75} S _{49.80}
	6	86.81	0.41	0.47	13.64	101.33	0.98	Pb _{49.64} Ag _{0.44} Sb _{0.45} S _{49.74}
	7	88.26	0.30	0.31	13.68	102.55	1.14	Pb _{49.64} Ag _{0.33} Sb _{0.29} S _{49.74}
	8	85.72	0.67	0.63	13.13	100.15	1.21	Pb _{49.56} Ag _{0.75} Sb _{0.62} S _{49.07}
	9	86.96	0.15	0.22	13.46	100.79	0.81	Pb _{49.81} Ag _{0.17} Sb _{0.21} S _{49.81}
	10	84.21	1.34	1.58	13.36	100.49	1.04	Pb _{47.90} Ag _{1.46} Sb _{1.53} S _{49.11}
	11	85.22	0.70	0.82	13.50	100.24	0.96	Pb _{48.63} Ag _{0.77} Sb _{0.80} S _{49.80}
	12	85.22	0.61	0.69	13.41	99.93	1.00	Pb _{48.91} Ag _{0.67} Sb _{0.67} S _{49.75}
	13	86.06	0.51	0.37	13.39	100.33	1.56	Pb _{49.41} Ag _{0.56} Sb _{0.36} S _{49.67}
	14	76.14	5.12	5.18	14.33	100.77	1.12	Pb _{40.63} Ag _{5.25} Sb _{4.70} S _{49.42}
	15	87.73	0.16	0.23	13.35	101.47	0.77	Pb _{50.22} Ag _{0.17} Sb _{0.22} S _{49.38}
Avg		86.54	0.83	0.88	13.60	101.21	1.06	Pb _{48.54} Ag _{0.88} Sb _{0.83} S _{49.68}
SA 12 M	1	87.37	0.14	0.16	13.54	101.20	1.00	Pb _{49.81} Ag _{0.15} Sb _{0.15} S _{49.88}
	2	86.08	0.17	0.18	13.15	99.58	0.94	Pb _{50.13} Ag _{0.19} Sb _{0.18} S _{49.50}
	3	87.04	0.17	0.15	13.50	100.86	1.11	Pb _{49.65} Ag _{0.56} Sb _{0.52} S _{49.27}
Avg		86.83	0.16	0.16	13.40	100.55	1.04	Pb _{49.81} Ag _{0.15} Sb _{0.15} S _{49.88}
J 19 550 S	1	87.01	0.51	0.53	13.36	101.42	0.96	Pb _{49.65} Ag _{0.56} Sb _{0.52} S _{49.27}
	2	86.18	0.35	0.51	13.30	100.34	0.68	Pb _{49.63} Ag _{0.38} Sb _{0.50} S _{49.48}
	3	85.92	0.36	0.41	13.50	100.19	0.87	Pb _{49.23} Ag _{0.39} Sb _{0.40} S _{49.97}
	4	82.87	1.61	1.72	13.07	99.27	0.94	Pb _{47.81} Ag _{1.78} Sb _{1.69} S _{48.71}
	5	85.97	0.41	0.41	13.22	100.01	0.99	Pb _{49.74} Ag _{0.45} Sb _{0.40} S _{49.41}
	6	86.32	0.31	0.33	13.04	99.99	0.93	Pb _{50.27} Ag _{0.34} Sb _{0.33} S _{49.07}
	7	85.95	0.36	0.33	12.85	99.49	1.09	Pb _{50.48} Ag _{0.41} Sb _{0.33} S _{48.78}
Avg		85.75	0.56	0.61	13.19	100.10	1.04	Pb _{49.54} Ag _{0.62} Sb _{0.60} S _{49.88}
EP 20 Q600S	1	87.39	0.04	0.18	13.40	101.01	0.28	Pb _{50.12} Ag _{0.05} Sb _{0.18} S _{49.65}
	2	86.55	0.22	0.24	13.12	100.12	1.00	Pb _{50.28} Ag _{0.24} Sb _{0.24} S _{49.24}
	3	87.12	0.17	0.20	13.14	100.62	1.00	Pb _{50.46} Ag _{0.19} Sb _{0.19} S _{49.16}
	4	85.96	0.19	0.22	13.34	99.71	1.00	Pb _{49.72} Ag _{0.21} Sb _{0.21} S _{49.86}
	5	85.50	0.13	0.28	13.07	98.98	0.52	Pb _{50.09} Ag _{0.14} Sb _{0.27} S _{49.49}
	6	86.20	0.14	0.23	13.21	99.79	0.70	Pb _{50.04} Ag _{0.16} Sb _{0.23} S _{49.57}
	7	86.99	0.27	0.34	13.21	100.81	0.91	Pb _{50.15} Ag _{0.30} Sb _{0.33} S _{49.22}
	8	86.66	0.18	0.23	13.35	100.42	1.48	Pb _{50.56} Ag _{0.31} Sb _{0.21} S _{48.92}
Avg		86.55	0.17	0.24	13.23	100.18	0.86	Pb _{50.18} Ag _{0.20} Sb _{0.23} S _{49.39}
EP 20 Q500S	1	87.40	0.28	0.21	13.09	100.98	1.53	Pb _{50.56} Ag _{0.32} Sb _{0.21} S _{48.92}
	2	87.71	0.23	0.16	13.71	101.81	1.50	Pb _{49.55} Ag _{0.24} Sb _{0.16} S _{50.05}
	3	87.88	0.17	0.21	13.48	101.73	0.90	Pb _{50.04} Ag _{0.18} Sb _{0.20} S _{49.58}
	4	87.79	0.19	0.27	13.69	101.94	0.77	Pb _{49.58} Ag _{0.20} Sb _{0.26} S _{49.96}
	5	87.66	0.19	0.29	13.41	101.54	0.75	Pb _{50.05} Ag _{0.21} Sb _{0.28} S _{49.46}
	6	87.60	0.11	0.15	13.30	101.16	0.86	Pb _{50.34} Ag _{0.12} Sb _{0.14} S _{49.40}
Avg		87.67	0.20	0.21	13.45	101.53	1.05	Pb _{50.02} Ag _{0.21} Sb _{0.21} S _{49.56}
EP 106 4Q2	1	88.07	0.13	0.13	13.94	102.27	1.08	Pb _{49.31} Ag _{0.14} Sb _{0.13} S _{50.42}
	2	87.73	0.30	0.15	13.62	101.80	2.36	Pb _{49.69} Ag _{0.33} Sb _{0.14} S _{49.84}
	3	87.14	0.13	0.20	13.69	101.16	0.74	Pb _{49.46} Ag _{0.14} Sb _{0.19} S _{50.21}
	4	87.42	0.24	0.13	13.58	101.37	2.00	Pb _{49.70} Ag _{0.26} Sb _{0.13} S _{49.91}
	5	88.37	0.11	0.16	13.74	102.37	0.80	Pb _{49.75} Ag _{0.12} Sb _{0.15} S _{49.97}
	6	87.56	0.23	0.12	13.57	101.47	2.08	Pb _{49.79} Ag _{0.25} Sb _{0.12} S _{49.85}
	7	88.81	0.14	0.19	13.86	103.01	0.83	Pb _{49.62} Ag _{0.15} Sb _{0.18} S _{50.05}
Avg		87.87	0.18	0.15	13.71	101.92	1.14	Pb _{49.62} Ag _{0.20} Sb _{0.15} S _{50.04}
CH 16 1	1	88.10	0.23	0.16	13.71	102.20	1.56	Pb _{49.93} Ag _{0.25} Sb _{0.16} S _{49.66}
	2	88.38	0.14	0.24	13.70	102.46	0.65	Pb _{49.78} Ag _{0.15} Sb _{0.23} S _{49.84}
	3	88.09	0.20	0.17	13.82	102.28	1.31	Pb _{49.47} Ag _{0.21} Sb _{0.16} S _{50.15}
	4	88.00	0.18	0.16	14.01	102.34	1.27	Pb _{49.12} Ag _{0.19} Sb _{0.15} S _{50.53}
	5	88.73	0.09	0.20	13.80	102.82	0.47	Pb _{49.73} Ag _{0.09} Sb _{0.19} S _{49.98}
	6	87.85	0.17	0.12	13.67	101.80	1.64	Pb _{49.72} Ag _{0.18} Sb _{0.11} S _{49.98}
	7	87.50	0.36	0.37	13.72	101.94	1.11	Pb _{49.32} Ag _{0.39} Sb _{0.35} S _{49.95}
	8	87.77	0.19	0.21	13.73	101.90	1.00	Pb _{49.52} Ag _{0.20} Sb _{0.20} S _{50.07}
	9	87.73	0.16	0.17	13.67	101.73	1.06	Pb _{49.81} Ag _{0.17} Sb _{0.16} S _{50.01}
	10	89.32	0.17	0.13	13.85	103.46	1.50	Pb _{49.81} Ag _{0.18} Sb _{0.12} S _{49.89}
Avg		88.15	0.19	0.19	13.77	102.29	1.16	Pb _{49.62} Ag _{0.20} Sb _{0.15} S _{50.01}

TABLE 3. (Cont.)

Sample no.	n	Pb	Ag	Sb	S	Total	Ag/Sb	Atomic formula
BT JN 19 CHM	1	86.45	0.17	0.15	13.62	100.39	1.20	Pb _{49.39} Ag _{0.18} Sb _{0.15} S _{50.29}
	2	87.58	0.08	0.10	13.53	101.29	0.90	Pb _{49.95} Ag _{0.09} Sb _{0.10} S _{49.86}
	3	87.72	0.20	0.18	13.40	101.50	1.22	Pb _{50.13} Ag _{0.22} Sb _{0.18} S _{49.48}
	4	86.80	0.14	0.13	13.41	100.47	1.15	Pb _{49.91} Ag _{0.15} Sb _{0.13} S _{49.81}
	5	86.97	0.21	0.19	13.59	100.96	1.21	Pb _{49.56} Ag _{0.23} Sb _{0.19} S _{50.03}
	6	86.77	0.17	0.18	13.60	100.72	1.12	Pb _{49.50} Ag _{0.19} Sb _{0.17} S _{50.14}
Avg		87.05	0.16	0.16	13.52	100.89	1.13	Pb _{49.74} Ag _{0.18} Sb _{0.15} S _{49.94}
EP 20 QUE	1	86.12	0.37	0.40	13.61	100.48	1.05	Pb _{49.09} Ag _{0.40} Sb _{0.35} S _{50.12}
	2	87.27	0.48	0.34	14.07	102.16	1.63	Pb _{48.57} Ag _{0.52} Sb _{0.32} S _{50.60}
	3	88.74	0.25	0.30	14.31	103.59	0.93	Pb _{48.71} Ag _{0.26} Sb _{0.28} S _{50.75}
	4	89.33	0.19	0.23	14.15	103.91	0.91	Pb _{49.20} Ag _{0.20} Sb _{0.22} S _{50.38}
	5	88.23	0.21	0.21	13.98	102.63	1.15	Pb _{49.21} Ag _{0.23} Sb _{0.20} S _{50.37}
Avg		87.94	0.30	0.29	14.02	102.55	1.13	Pb _{49.96} Ag _{0.32} Sb _{0.28} S _{50.44}
2EP 19 BXC	1	87.47	0.26	0.20	13.63	102.55	1.47	Pb _{49.60} Ag _{0.28} Sb _{0.19} S _{49.93}
	2	86.29	0.19	0.19	13.50	100.16	1.11	Pb _{49.53} Ag _{0.20} Sb _{0.18} S _{50.08}
	3	87.43	0.13	0.15	14.02	101.74	0.93	Pb _{48.97} Ag _{0.14} Sb _{0.15} S _{50.74}
	4	87.05	0.86	1.00	13.88	102.78	0.97	Pb _{48.34} Ag _{0.91} Sb _{0.94} S _{49.81}
	5	88.14	0.18	0.27	13.85	102.44	0.80	Pb _{49.39} Ag _{0.20} Sb _{0.25} S _{50.16}
Avg		87.27	0.32	0.36	13.78	101.94	1.06	Pb _{49.17} Ag _{0.35} Sb _{0.34} S _{50.14}

Operating conditions: 15kV, 30nA, 2 micron beam, 15-s count time; lines: S K α ; Pb M α ; Ag L α ; Sb L α

in silver sulfide and sulfosalt minerals more common in the upper workings (Megaw, 1990) in addition to incorporation into the solid solution. However, no other silver phases were noted in the microprobe analyses.

Galena compositions and district zoning

Mineralogic zonation at the San Antonio mine was suggested by Bond (1986) to consist of arsenopyrite, pyrrhotite,

and chalcopyrite, increasing in abundance with depth and galena, displaying the opposite trend. Lead and antimony show geochemical zonation, with concentrations in ores increasing toward the surface, whereas arsenic, bismuth, silver, and selenium increase with depth. Metal ratios determined by Bond (1986) and Walter (1985) show increases in Ag/Pb and Cu/Ag with depth, with a decrease in Ag/Zn, Pb/Zn, Pb/Cu, Pb/Bi, and Sb/Bi. These variations in chemistry are based on bulk ore analysis not obviously reflected in galena compositions at the San Antonio mine with respect to Ag, Sb, As, or Se. High Bi values (174–665 ppm Bi) reported by Bond (1986) from level 14 correspond to an occurrence of Bi-bearing galena solid solution (0.8 wt % in galena) from the same level. Overall, bismuth-bearing galena is only observed in skarn ores and not in mantos. Malakov (1968) noted distinct differences in galena compositions (with respect to Bi and Sb) between deposit types. Galenas from skarn deposits are more commonly Bi rich compared to vein or replacement types where Sb is more common. In the East camp, bismuth-bearing galenas are restricted to the skarns. Amcoff (1984) reviewed the solubility of Ag-Sb,Bi in galena and found that Ag-Bi is more soluble than Ag-Sb coupled solid solution at any temperature, a feature also observed by Foord and Shawe (1988). The rare occurrence of Bi in galena at Santa Eulalia may reflect the low concentrations of the element in the ore fluid throughout the district. The exclusive occurrence of bismuth in skarn reflects early precipitation in higher temperature skarn ores. Antimony displays a similar behavior. Comparison of galena samples from level 8 from skarn (4.2 at. % Sb) and manto (2.5 at. % Sb) reveals that the highest antimony values are in skarn ores. This relationship implies a temperature and/or wall-rock control on the distribution of antimony in galena.

Megaw (1990) noted a lack of metal zonation within individual orebodies in the West camp, yet determined that large-scale variations occur within that portion of the district.

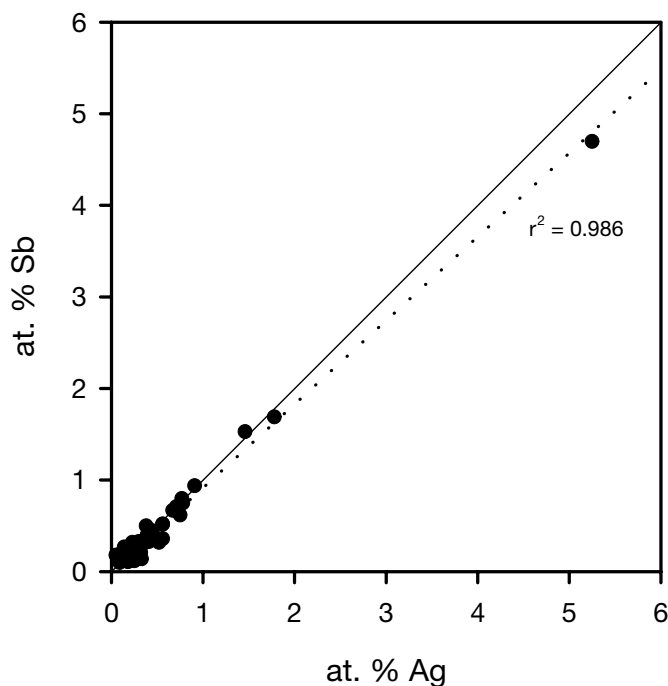


FIG. 8. Ag and Sb concentrations in galena determined by electron microprobe analysis. Solid line represents a theoretical 1/1 coupled substitution. Dashed line represents a regression line fit to the data, with an r value of 0.986.

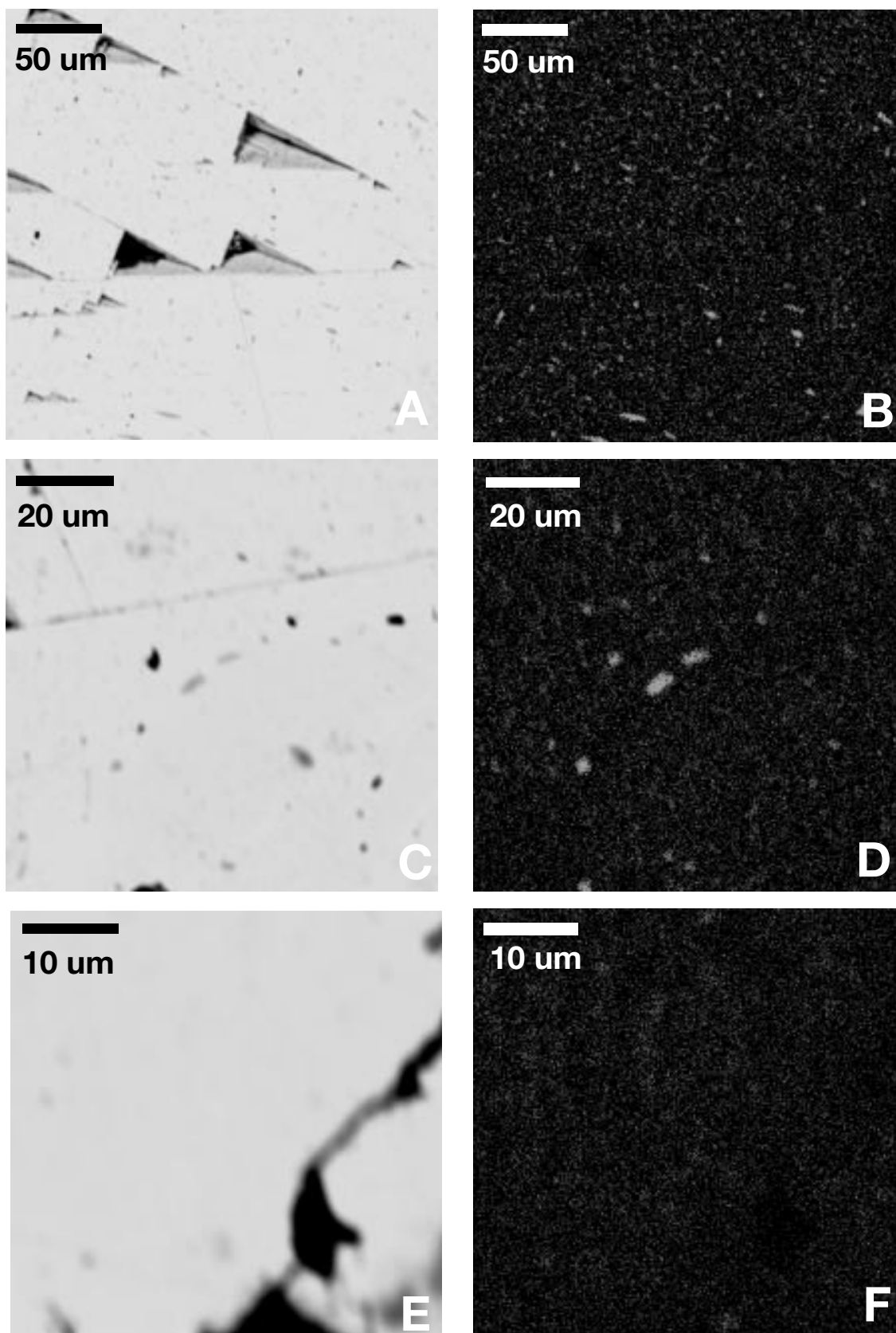


FIG. 9. Backscatter and silver X-ray maps of different zones in a single galena crystal from the West camp of Santa Eulalia. A and B are from the core zone of the galena crystal. C and D are from the rim-core transition zone. E and F are from the grain rim.

Prescott (1916) also noted a broad metals zonation. The northern West camp ores are higher in Ag, Fe, and Si and poorer in As, Pb, and Zn compared to the southern orebodies. A large-scale variation is also apparent in silver and antimony contents of galena from the West camp. Silver and antimony values (Table 1) are consistently higher near the Condesa fracture (mean = 2.8 at. % in galena, 1.1σ) than in samples from the Central West camp (mean = 1.8 at. % in galena, 0.6σ). Metal ratios in the West camp are relatively consistent within orebodies (Aguirre, 1987), although they vary slightly between individual orebodies, a feature also seen in galena compositions. Ag/Sb ratios tend to be higher for samples from the silicate orebodies and lower in the chimneys and breccias. Megaw (1990) also noted that Ag/Pb ratios are also greater in these areas.

Galena compositions and temperature

Comparison to fluid inclusion data: Fluid inclusion temperatures of Megaw (1990) show a 150°C range across the district (filling temperatures in fluorite = 200°–350°C). However, he noted that the distribution of fluid inclusion data points was insufficient to document a temperature gradient. Although two fluids were identified by Megaw (1990), based on salinity differences, filling temperatures were similar.

The lack of obvious temperature gradients at Santa Eulalia, as documented by fluid inclusion filling temperatures, is problematic considering the degree of compositional variation in the galena solid solution. Significant variations in galena compositions require some physiochemical control in light of the work done in the Ag-Sb-Pb-S system by previous investigators. Amcoff (1976) and Foord and Shawe (1988) noted a strong correlation between Ag-Sb, Bi substitution and temperature for galena solid solution. Higher temperatures favor solid-solution formation while low temperatures inhibit miscibility of Ag and Sb in PbS. Annealing experiments using silver-antimony galenas from Wood River, Idaho (Hall and Czamanske, 1972), indicated the galena was deposited as a single phase (solid solution) in the system $(\text{PbS})_2\text{-}\beta\text{AgSbS}_2$ within a temperature range of 350° to 400°C, based on the disappearance of microinclusions. These temperatures represent the upper end of fluid inclusion temperatures determined by Megaw (1990). Comparing the variation in Ag and Sb concentrations to experimental data of Amcoff (1976), a maximum solid solution of 5 at. percent would correspond to a deposition temperature of approximately 300°C. Low Ag-Sb galena (2 at. % Ag or Sb) corresponds to crystallization temperatures below 217°C. Ag-Sb substitution is strongest in the deepest portions of the West camp, perhaps reflecting temperature control near inferred fluid sources.

Very low thermal gradients of 8° and 25°C/km have been documented in replacement-skarn systems by Buseck (1966) and Meinert (1987). The fluid inclusion data reported by previous workers in the Santa Eulalia district is not precise enough to resolve such subtle variation. The ore fluids traveled significant distances through limestone before ore deposition began. Megaw (1990) cited the experimental work of Hemley et al. (1986) that illustrated that metal chloride solubilities increase with decreasing pressure and near constant temperatures. More recent hydrothermal models which incorporate changing temperature and pressure considerations

or other chemical variables (e.g., Hemley and Hunt, 1992) also allow for distant migration of ore fluids and appear to accommodate many of the mineralization features observed at Santa Eulalia. Previous workers noted that precipitation of ore minerals did not begin until the felsite dikes and sills breached the diabase sills (Fig. 3), perhaps coinciding with a thermal boundary (Hewitt, 1968; Megaw 1990).

Comparison to sulfur isotope data: The silver and antimony variation determined by this study correlates with sulfur isotope variation in the West camp. Megaw (1990) noted a sulfur isotope zonation in the West camp, which is not present in the East camp. The lack of paragenetic control due to the telescoped and overprinted mineralization patterns in the East camp inhibit the recognition of any zoning. However, the range in values between the two camps is virtually identical, although the values are more positive in the East camp. The variation in sulfur isotope compositions for the West camp is over 15 per mil (Table 1). The lowest isotopic values are found in the Condesa fracture, which also exhibits the highest Ag and Sb values. The highest isotopic values are from the central West camp, an area of low to moderate Ag and Sb values in galena. Within a particular area of mineralization, e.g., the Condesa fracture, coupled silver-antimony substitution is readily apparent as are the variations in galena Ag/Sb ratios from depth to the surface. The sulfur isotope zonation, galena Ag-Sb substitution, and galena Ag/Sb ratios all appear to reflect distance from inferred fluid sources. This variation may be due to temperature gradients, modified by changing sulfur/metal ratios, which resulted in the isotopic disequilibrium between sulfide species (Ohmoto, 1972), a feature noted at Santa Eulalia by Megaw (1990). Temperature calculations based on equilibrium pairs of sphalerite and galena range from 268° to 477°C. These values overlap those of the fluid inclusion determinations.

East camp sulfur isotope values display a wide range over relative short distances. Megaw (1990) attributed this to higher concentrations of dissolved sulfur species (m_{S_2}) compared to the West camp where the isotopic range is similar (although more negative) and spread out over greater distances. The higher East camp sulfur isotope values probably reflect the superimposed nature of the mineralization with higher dissolved sulfur concentrations (Ohmoto, 1972). Direct comparison of sulfur isotopes and galena compositions, between skarn and manto ores, reveals a distinct shift in $\delta^{34}\text{S}$ and Ag-Sb concentrations in galena between samples that display isotopic equilibrium between galena and sphalerite. High Ag-Sb galena in skarn (Ag = 4.3 at. %; Sb = 4.2 at. %) on level 8 has lower $\delta^{34}\text{S}$ values (-10.57‰) when compared to manto ore on the same level (Ag = 2.2 at. %, Sb = 2.5 at. %, and $\delta^{34}\text{S} = -3.29\text{‰}$). This relationship suggests that skarn ores reflect higher temperatures of formation compared to the manto replacement ores, a feature noted by Malakov (1968), when comparing galena compositions in diverse ore types. The shift in sulfur isotope values also reflects a marked difference between skarn and connected manto ores.

In the West camp, both sulfur isotopes and galena solid solutions vary systematically. Comparison of $\delta^{34}\text{S}$ values to at. percent Sb (or Ag) in galena reveals an inverse slope for samples along a given flow path (e.g., Condesa trend, Fig. 10). High antimony contents have correspondingly low $\delta^{34}\text{S}$ values.

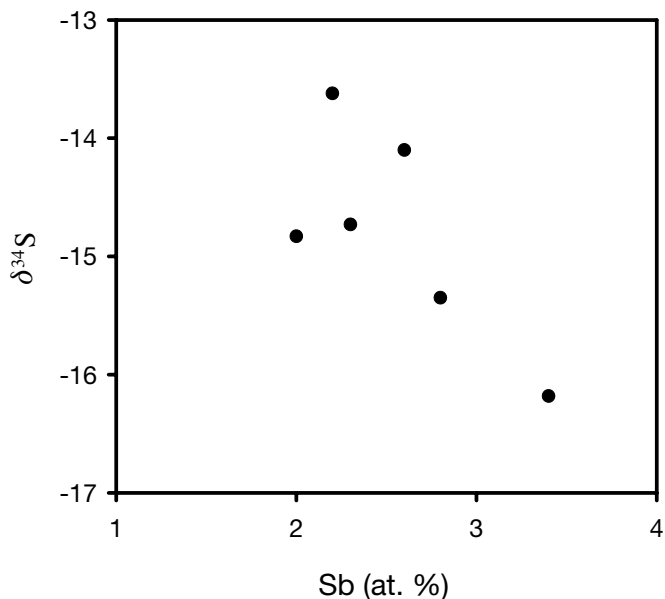


FIG. 10. Comparison of sulfur isotope values for galena to antimony concentration in the same sample from the Condesa breccia region, West camp, Santa Eulalia.

Fractionation of sulfur isotopes and increasing silver-antimony contents of galena appear to reveal evidence of fluid evolution. This relationship holds to a lesser degree for samples from other parts of the West camp. The cause for this observed variation remains speculative, but may be due to temperature, pressure, and/or changing metal or nonmetal activities.

Galena compositions and fluid evolution

The apparent lack of bismuth and copper in the ores did not allow the formation of other sulfosalt phases (Amcoff, 1976; Foord and Shawe, 1988). In addition, the overall system lacks evidence of strong temperature or pressure gradients (which result in boiling) that lead to the formation of bonanza-type silver sulfosalt deposition in volcanic-epithermal systems (Lueth et al., 1990). Only the Condesa breccia and Tunel orebodies show good evidence for intramineral explosive brecciation, analogous to the pressure release in epithermal systems. These two areas are also the only areas in the district to contain significant amounts of sulfosalts. The combination of low Bi and Cu concentrations and subtle temperature-pressure gradients resulted in the partitioning of silver and antimony into galena rather than the formation of discrete Ag-Pb-Bi-Sb sulfosalt phases. The partitioning of Ag and Sb into galena occurred gradually and over large distances and appears to encode evidence of fluid evolution as a response to temperature, pressure, and/or fluid fractionation across the West camp of the district. This relationship is best seen along the Condesa chimney by comparing Sb or Ag to distance from the Condesa Felsite (Fig. 11). The highest concentrations are observed near the felsite, the source of the ore fluids inferred by Megaw (1990). A similar variation in Ag/Sb ratios in the galena compositions may reflect variable activities of the solid-solution components as a response to temperature, fractionation, and/or wall-rock interaction (normal

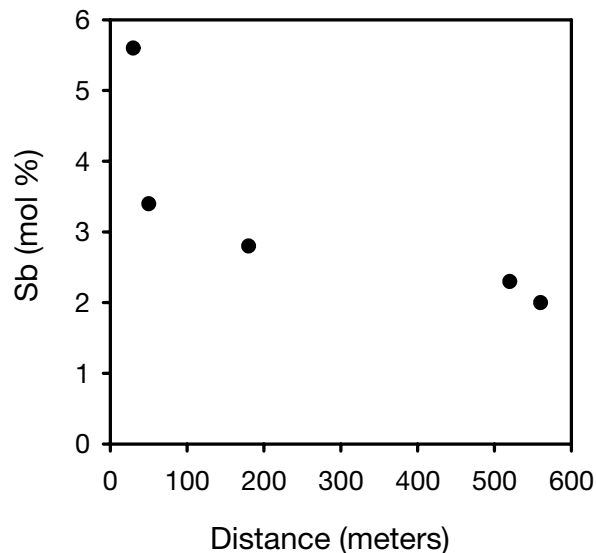


FIG. 11. Antimony concentrations in galena compared to distance from the Condesa Felsite for samples in the Condesa breccia region, West camp, Santa Eulalia.

sulfides deep compared to silicate ores nearer to the surface). The more chaotic distribution of Ag and Sb in the East camp reflects telescoped mineralization. The inclusion-rich zones in some galena grains are apparently argentiferous pockets formed by earlier or more primitive batches of hydrothermal fluid and ultimately were overgrown by galena precipitated from more evolved fluids.

Summary

Coupled substitution of Ag-Sb for Pb can explain most of the distribution of Ag and Sb in argentiferous galena from the Santa Eulalia district. Variations in both the Ag/Sb and (Ag + Sb)/Pb ratios are noted between individual orebodies and along inferred flow directions for the mineralizing fluids. These small variations are consistent with mineralogical and geochemical zoning patterns in the district. Variations in the composition of the galena solid solution and sulfur isotope values reflect temperature and/or chemical gradients, although mineralization temperatures are only partly constrained by fluid inclusion-derived temperatures.

Acknowledgments

We would like to acknowledge the thoughtful and constructive reviews of Steven Scott and David Huston. Bill Chavez and the late Eugene Foord also provided constructive suggestions concerning early versions of the manuscript. Guy Crawford, University of Texas at El Paso (UTEP), assisted in the DCP-AES analysis of the galena. Nelia Dunbar, New Mexico Institute of Mining and Technology (NMIMT) assisted with the backscatter and X-ray map electron microprobe analysis. Leo Gabaldon and Kathy Glesener, New Mexico Bureau of Mines and Mineral Resources (NMBMMR), drafted some of the figures.

This material is based on work supported by the National Science Foundation (NSF) under grant USE-9251116 to V.W.L. The electron microprobe laboratory facility at UTEP

was funded by NSF grant RII-8504371 and the Permanent University Fund of the University of Texas system. The Cameca SX-100 electron microprobe at NMIMT was partially funded by an NSF grant STI-9413900.

July 13, 1999; June 10, 2000

REFERENCES

- Aguirre, E.F. de J., 1987, Determinacion del sonamiento en las chimeneas de la Mina Buena Tierra, a partir de los cocientes metalicos: Unpublished Professional thesis, Mexico, University of Guanajuato, 40 p.
- Amcoff, Ö., 1976, The solubility of silver and antimony in galena: Neues Jahrbuch für Mineralogie Monatshefte, v. 6, p. 247–261.
- 1984, Distribution of silver in massive sulfide ores: Mineralium Deposita, v. 19, p. 63–69.
- Bond, B.R., 1986, Mineralogical and geochemical zoning, San Antonio mine, Santa Eulalia mining district, Chihuahua, Mexico, in Clark, K.F., Megaw, P.K.M., and Ruiz, J., eds., Lead-zinc-silver carbonate-hosted deposits of northern Mexico: Littleton, CO, Society of Economic Geologists, p. 233–253.
- Buseck, P.R., 1966, Contact metasomatism and ore deposition—Concepcion del Oro, Mexico: ECONOMIC GEOLOGY, v. 61, p. 97–136.
- Foord, E.E., and Shawe, D.R., 1988, The Pb-Bi-Ag-Cu(Hg) chemistry of galena and some associated sulfosalts: A review and some new data from Colorado, California, and Pennsylvania: Canadian Mineralogist, v. 26, p. 251–268.
- Foord, E.E., Shawe, D.R., and Concklin, N.M., 1988, Coexisting galena, PbS, and sulfosalts: Evidence for multiple episodes of mineralization in the Round Mountain and Manhattan gold districts, Nevada: Canadian Mineralogist, v. 26, p. 355–376.
- Hall, W.E., and Czamanske, G.K., 1972, Mineralogy and trace element content of the Wood River lead-silver deposits, Blaine County, Idaho: ECONOMIC GEOLOGY, v. 67, p. 350–361.
- Hemley, J.J., and Hunt J.P., 1992, Hydrothermal ore-forming processes in light of studies in rock-buffered systems: II. Some general geologic applications: ECONOMIC GEOLOGY, v. 87, p. 23–43.
- Hemley, J.J., Cygan, G.L., and d'Angelo, W.M., 1986, Effect of pressure on ore mineral solubilities under hydrothermal conditions: Geology, v. 14, p. 377–379.
- Hewitt, W.P., 1943, Geology and mineralization of the San Antonio mine, Santa Eulalia district, Chihuahua, Mexico: Geological Society of America Bulletin, v. 64, p. 173–204.
- 1968, Geology and mineralization of the Main mineral zone of the Santa Eulalia district, Chihuahua, Mexico: American Institute of Mining Engineers Transactions, v. 240, p. 229–260.
- Hoda, S.N., and Chang, L.L.Y., 1975, Phase relations in the systems PbS-Ag₂Sb₂S₃ and PbS-Ag₂S-Bi₂S₃: American Mineralogist, v. 60, p. 621–633.
- Lueth, V.W., Goodell, P.C., and Pingitore, N.E., Jr., 1990, Encoding the evolution of ore system in bismuthinite-stibnite compositions, Julcani, Peru: ECONOMIC GEOLOGY, v. 85, p. 1462–1472.
- Lueth, V.W., Megaw, P.K.M., Pingitore, N.E., and Goodell, P.C., 1996, Compositional study of argentiferous galena from the West camp of the Santa Eulalia mining district: Conferencia Internacional de Minera-Excursion geologica al Cenozoico de Chihuahua, 6th, 1996, Facultad de Ingenieria Universidad Autónoma Chapingo-Mexican Geological Society-Colegio de Ingenieros Geologos de Mexico A.C., Proceedings, p. 63–73.
- Malakhov, A.A., 1968, Bismuth and antimony in galenas as indicators of some conditions of ore formation: Geochemistry International, v. 7, p. 1055–1068.
- Megaw, P.K.M., 1986a, Mineralogy of the Santa Eulalia mining district, Chihuahua, Mexico: Rochester Academy of Science Mineral Symposium, 13th, April 10–13, 1986, Proceedings, p. 21–31.
- 1986b, Geology and geologic history of the Santa Eulalia mining district, Chihuahua, Mexico, in Clark, K.F., Megaw, P.K.M., and Ruiz, J., eds., Lead-zinc-silver carbonate-hosted deposits of northern Mexico: Littleton, CO, Society of Economic Geologists Guidebook Series, p. 179–212.
- 1990, Geology and geochemistry of the Santa Eulalia mining district, Chihuahua, Mexico: Unpublished Ph.D. dissertation, Tucson, AZ, University of Arizona, 461 p.
- Megaw, P.K.M., Ruiz, J., and Titley, S.R., 1988, High-temperature, carbonate-hosted, Pb-Zn-Ag massive sulfide deposits of Mexico: ECONOMIC GEOLOGY, v. 83, p. 1856–1885.
- Meinert, L.D., 1987, Skarn zonation and fluid evolution in the Groundhog mine, Central mining district, New Mexico: ECONOMIC GEOLOGY, v. 82, p. 523–545.
- Ohmoto, H., 1972, Systematics of sulfur and carbon isotopes in hydrothermal ore deposits: ECONOMIC GEOLOGY, v. 67, p. 551–579.
- Pouchou, J.L., and Pichoir, F., 1984, A new model for quantitative X-ray microanalysis, Part I. Application to the analysis of homogeneous samples: Recherche Aerospatiale, v. 25, p. 393–399.
- Prescott, B. 1916, The main mineral zone of the Santa Eulalia district: American Institute of Mining Engineers Transactions, v. 51, p. 57–99.
- 1926, The underlying principles of the limestone replacement deposits of the Mexican province: Engineering and Mining Journal, v. 122, p. 246–253.
- Rubeska, I., Sulcek, Z., and Moldan, B., 1967, The determination of silver in sulphide minerals by atomic absorption spectrophotometry: Analytica Chimica Acta., v. 37, p. 27–32.
- Sharp, T.G., and Buseck, P.R., 1993, The distribution of Ag and Sb in galena: Inclusions versus solid solution: American Mineralogist, v. 78, p. 85–95.
- Sharp, T.G., Zheng, N.J., Tsong, I.S.T., and Buseck, P.R., 1990, Scanning tunneling microscopy of defects in Ag- and Sb-bearing galena: American Mineralogist, v. 75, p. 1438–1442.
- Van Hook, H.J., 1960, The ternary system Ag₂S-Bi₂S₃-PbS: ECONOMIC GEOLOGY, v. 55, p. 759–788.
- Walter, T.G., 1985, Metals distribution at the San Antonio mine, Santa Eulalia mining district, Chihuahua, Mexico: Unpublished M.S. thesis, Tucson, AZ, University of Arizona, 102 p.

